

Copyright 2016, ABRACO

Trabalho apresentado durante o INTERCORR 2016, em Búzios/RJ no mês de maio de 2016.

As informações e opiniões contidas neste trabalho são de exclusiva responsabilidade do(s) autor(es).

## **EIS and Salt-Spray study of AA2524 anodized in tartaric-sulfuric acid bath and protected with hybrid sol-gel coating**

Hellen Costenaro<sup>1</sup>, Fernanda M. Queiroz<sup>2</sup>, Maysa Terada<sup>3</sup>, Yoann Paint<sup>4</sup>, Alexis Renaud<sup>5</sup>, Marie-George Olivier<sup>6</sup>, Isolda Costa<sup>7</sup>, Hercílio G. de Melo<sup>8</sup>

### **Abstract**

AA2524 is a relatively new brand of aluminum alloy designed to build lightweight structural components in aerospace industry. To be employed in aircrafts, high strength Al alloys need to be protected from corrosion by a robust protection system. One of the steps applied in the protection protocol is anodizing, which is known to greatly improve the corrosion resistance of Al alloys. In the present investigation, a sol-gel hybrid layer was applied as a post-treatment step for anodized AA2524 and the corrosion resistance of the system evaluated by means of EIS measurements and salt-spray tests. The anodizing process was performed in a tartaric-sulfuric acid (TSA) bath, which is more environmentally friendly than the traditional chromic acid anodizing baths, and the sol-gel solution was prepared by mixing tetraethoxysilane (TEOS) and 3-glycidioxypropyl-trimethoxysilane (GPTMS) precursors in a solution with high water content. For comparison reasons, TSA anodized samples were also hydrothermally sealed in boiling deionized water. The results of both EIS and salt-spray tests demonstrated superior corrosion resistance for the anodized samples post-treated with the hybrid sol-gel layer. Electrical equivalent circuit fitting of the EIS data indicated that the hybrid sol-gel layer strongly hinders electrolyte penetration through the porous layer, better protecting the underlying substrate.

**Keywords:** AA2524, anodizing process, hybrid sol-gel coatings, corrosion protection.

---

<sup>1</sup> Master, Chemical Engineer, PhD student, Polytechnic School of the University of São Paulo, University of Mons.

<sup>2</sup> PhD, Chemical Engineer, post-doctoral student, Polytechnic School of the University of São Paulo.

<sup>3</sup> PhD, Materials Engineer, post-doctoral student, Polytechnic School of the University of São Paulo.

<sup>4</sup> Master, Research assistant, Materia Nova Research Center.

<sup>5</sup> Master, Chemical engineer, PHD student, University of Mons.

<sup>6</sup> PhD, Professor, Faculty of Engineering, University of Mons, Materia Nova Research Center.

<sup>7</sup> PhD, Professor, Nuclear and Energy Research Institute.

<sup>8</sup> PhD, Professor, Polytechnic School of the University of São Paulo.

---

<sup>a</sup> Mestre, Engenheiro de Petróleo - EMPRESA A

<sup>b</sup> Engenheiro Civil - EMPRESA B

<sup>c</sup> PHD, Engenheira Civil - EMPRESA C

## 1 - Introduction

Aluminum alloys, such as AA2524, are extensively used for lightweight structures components in aerospace industry, where the combination of high specific strength and durability is essential (1) (2). However, due to their complex microstructure, these alloys are very sensitive to localized corrosion in chloride environments making necessary the use of protective treatments in order to maintain their integrity (3).

One of the protection methodologies consists of thickening the aluminum oxide film by anodizing, which, due to its particular structure (composed of a thin barrier layer and a thick porous layer), provides both corrosion resistance and a base layer for applying a protective organic coating. Anodizing is accomplished through an electrochemical reaction in acidic electrolytes (4) (5). Chromium based anodizing has been widely utilized and is the most efficient system for aluminum alloys, but hexavalent chromium species are known to be toxic and hazardous, which has led to the replacement of chromium and the implementation of alternative chromium-free anodizing electrolytes (6). One of these processes is the tartaric-sulfuric acid (TSA) anodizing, which is considered environmentally suitable and provides good corrosion resistance for aerospace alloys with appropriate paint adhesion (7).

In the aircraft industry, for an effective protection, the anodized layer must be painted or sealed (4) to prevent penetration of aggressive species to the base metal. Sealing using  $\text{Cr}^{6+}$  compounds has been used, providing excellent corrosion resistance, but its use has been increasingly banned forcing alternative chemistries to be adopted (1).

Sol-gel coatings have been studied as potential environmentally benign surface paint pre-treatments for aluminum alloys and has demonstrated to be an efficient alternative for the replacement of the chromate technology (8).

The aim of this work is to investigate the corrosion resistance of TSA anodized AA2524 protected with a hybrid organic-inorganic sol-gel layer with the purpose of improving the corrosion resistance while maintaining the future compatibility with organic coatings. For comparison, TSA anodized specimens unsealed and hydrothermally sealed in deionized boiling water were also tested. This latter treatment is recognized to improve the corrosion resistance of anodized Al alloys; however, it cannot be used prior to organic coating application due to its poor adhesion properties. The corrosion behavior was evaluated in NaCl 0.1 mol.L<sup>-1</sup> solution by EIS as a function of immersion time, and by salt-spray test until samples failure.

## 2. - Methodology

The AA2524 specimens were kindly supplied by EMBRAER S.A. The chemical composition of the alloy is 4.07 wt.% Cu, 1.66 wt.% Mg, 0.60 wt.% Mn, 0.10 wt.% Zn, 0.11 wt.% Fe, 0.03 wt.% Ti, 0.01 wt.% Si and 0.02 wt.% others.

Prior to anodizing, specimens with dimensions 4.5 cm x 5.0 cm x 0.105 cm were degreased by sonication in acetone for 10 min. The surface treatment was performed by dipping the samples in an alkaline etching solution: NaOH (40 g.L<sup>-1</sup>) at 40 °C for 30 s and in a chromate-free commercial acid dismutting bath (Turco<sup>®</sup> Smuttgo-Henkel) at room temperature for 15 s.

Between each step of surface preparation the specimens were thoroughly washed with distilled water.

Samples were anodized in a tartaric-sulfuric acid bath (TSA) ( $40 \text{ g.L}^{-1} \text{ H}_2\text{SO}_4$  and  $80 \text{ g.L}^{-1} \text{ C}_4\text{H}_6\text{O}_6$ ) at 14 V for 20 min at 37 °C.

After the anodizing step, the specimens were immediately rinsed with distilled water and hydrothermally sealed in boiling deionized water for 40 min or coated with a hybrid organic–inorganic sol–gel layer using a KSV Nima dip-coater for 2 min with withdrawal speed fixed of  $100 \text{ mm.min}^{-1}$  and afterwards cured at 150 °C for 1 h in a furnace.

The sol–gel solution was prepared by addition of tetraethoxysilane (TEOS) (20 % v/v) and 3-glycidyloxypropyl-trimethoxysilane (GPTMS) (10 % v/v) in a mixture of ethanol (10 % v/v) and distilled water (58 % v/v). The pH was adjusted with acetic acid in a continuously stirred sol-gel solution to 2.3-2.5. All chemicals were of analytical grade and used as received.

The FE-SEM investigation was performed using a Hitachi SU8020 microscope coupled to an energy dispersive X-ray spectrometer analyzer (EDX).

For the EIS tests a Princeton Applied Research Parstat 2273 (Ametek) potentiostat-frequency response analyzer system controlled by the Power Suite<sup>®</sup> software was used. EIS was carried out in a classical three electrodes arrangement using a  $7.07 \text{ cm}^2$  area of the specimen as working electrode, Ag/AgCl (+0.207 V vs. SHE) as reference electrode and platinum plate as counter electrode.

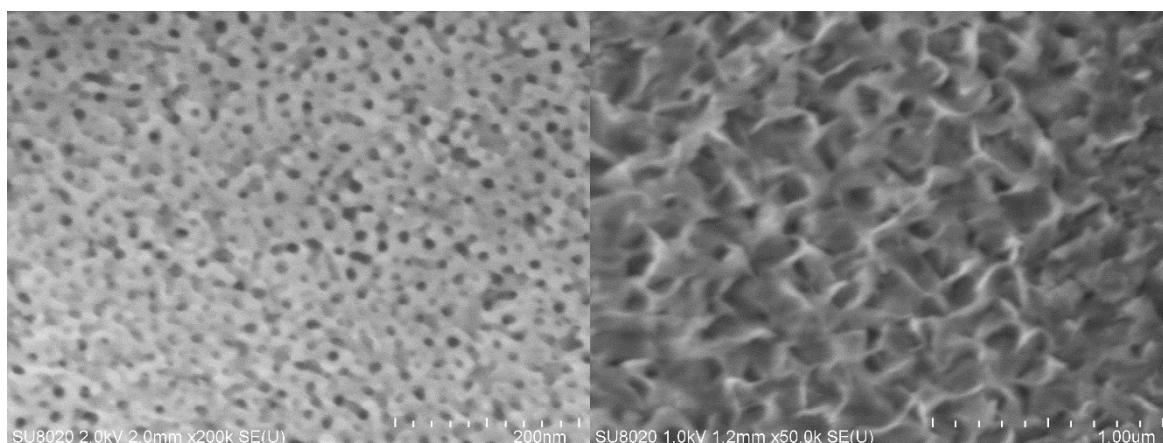
EIS measurements were taken after different immersion times at room temperature, in a naturally aerated  $0.1 \text{ mol.L}^{-1} \text{ NaCl}$  solution, over a frequency range from  $10^5$  to  $10^{-2} \text{ Hz}$  with 10 points per decade using an ac signal amplitude of 20 mV (rms). The test lasted 1008 h, corresponding to 42 days.

The salt-spray tests were conducted according to standard ASTM B117-11 (9) using a salt spray chamber Q-FOG Cyclic Corrosion Tester. For control and detection of corrosion initiation, samples were observed after 6 h, 24 h, 48 h, 72 h, 96 h, 168 h, 240 h and 336 h of test initiation.

### 3 - Results and discussion

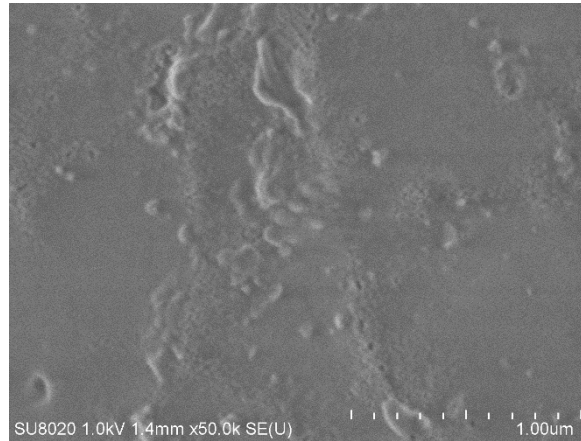
#### 3.1 - Morphological characterization

Figure 1 shows SEM micrographs of the top surfaces of unsealed (a), hydrothermally sealed (b) and hybrid sol–gel coated (c) TSA anodized layers.



(a) Unsealed

(b) hydrothermally sealed



(c) coated with hybrid sol-gel layer

**Figure 1 – Top surface SEM micrographs of TSA anodized AA2524 samples: (a) unsealed, (b) hydrothermally sealed for 40 min and (c) coated with the hybrid sol-gel**

In Figure 1 (a) it is possible to observe the porous structure of the anodized layer. The pore morphology is irregular, characteristic of Al–Cu alloys, which is ascribed to copper enrichment in the substrate surface during the anodizing procedure, incorporation of copper species into the anodic film and oxygen generation (10). The porosity obtained was close to 31 % and the pore diameter around 12 nm. From the cross section image of TSA anodized sample (Fig.2) it was possible to determine the thickness of the anodic layer as approximately 3.24  $\mu\text{m}$ . This value is similar to those reported by Capellosi *et al.* (4) and Boisier *et al.* (11) for clad and bare AA2024, respectively. The layer also seems to be compact, uniform and adherent to the substrate surface.

The hydrothermally sealed sample (Fig 1(b)) clearly shows the growth of “petal-shaped” crystals on the surface, denominated smudge, being in good agreement with the literature (11). The initial porous structure disappears as a result of the dissolution of the porous wall, followed by the diffusion and precipitation of aluminum hydroxide during the sealing process. The precipitation of aluminum hydroxide plugs the upper part of the pores, preventing environmental access to the barrier layer and increasing the corrosion resistance (11) (12).

Figure 1 (c) shows a non-homogenous surface for the sample coated by the hybrid sol-gel. It is possible to see that the hybrid layer did not cover some pores. One possible explanation is that the hybrid sol-gel penetrates through the porous layer but do not fill all the pore thickness. Further investigations have to be done to verify if the hybrid is present inside the pores through the entire anodic layer thickness.

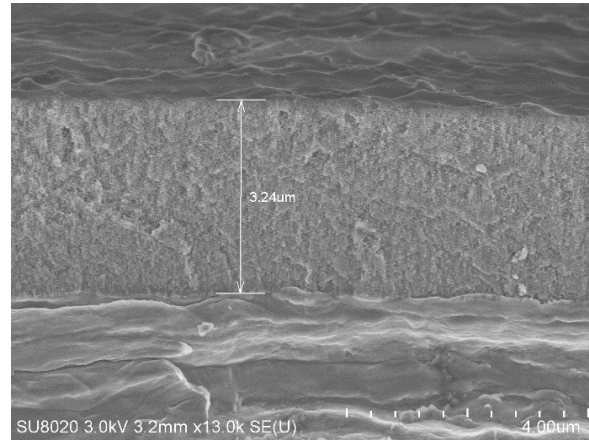


**Figure 2 – SEM cross section micrograph of unsealed TSA anodized layer on AA2524. Anodizing voltage: 14 V**

### 3.2 - Electrochemical characterization

#### 3.2.1 - EIS of unsealed TSA anodized AA2524

Figure 3 shows EIS diagrams for unsealed TSA anodized AA2524 as a function of immersion time in  $0.1 \text{ mol.L}^{-1}$  NaCl solution.

Two time constants can be observed in the Bode diagrams of Figure 3. The one at high frequencies is related to the porous layer, whereas at lower frequencies the time constant is attributed to the barrier layer, which is responsible for the effective corrosion resistance of the system (4) (11). For all the tests performed, after 72 h of immersion, the AA 2524 unsealed samples surfaces were corroded and the EIS measurements were interrupted.

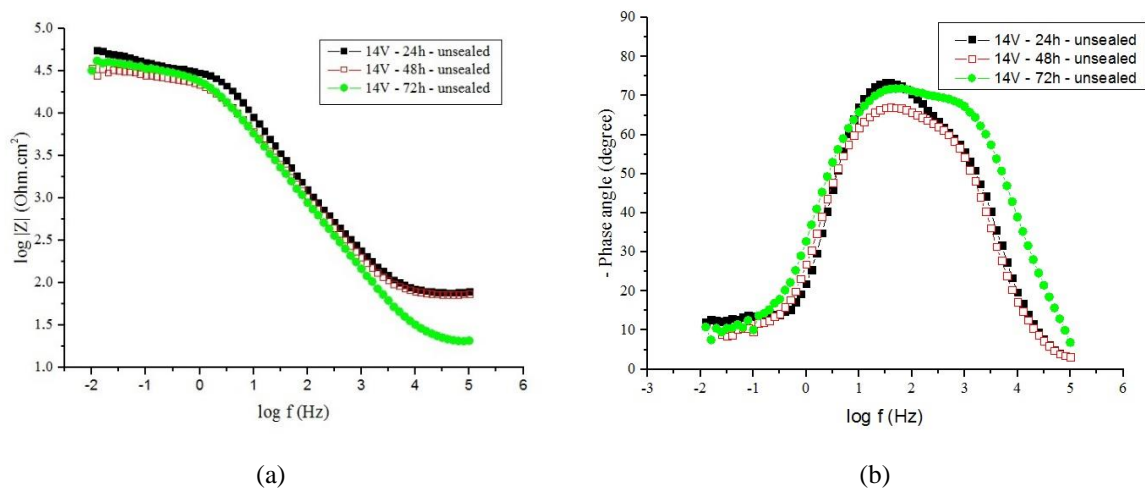


**Figure 3 - Bode plots in (a) Z modulus and in (b) phase angle for unsealed TSA anodized AA2524 after different immersion times in a  $0.1 \text{ mol.L}^{-1}$  NaCl solution**

An equivalent electrical circuit (EEC) was proposed to fit the experimental EIS data of the unsealed TSA anodized AA2524 for 24 h, 48 h and 72 h of immersion in  $0.1 \text{ mol.L}^{-1}$  NaCl solution (Fig. 4). The heterogeneities in the barrier and porous layers led to the use of constant

phase elements (CPE) rather than simple capacitances (C) to fit the experimental data. The porous layer is represented by the pore resistance  $R_p$ , which is in parallel with the porous layer capacitance,  $CPE_p$ , whereas the barrier layer properties are represented by its resistance,  $R_b$ , in series with its capacitance,  $CPE_b$ . Table 1 shows the values of the fitted parameters for  $R_b$ ,  $CPE_b$ ,  $n_b$ ,  $R_p$ ,  $CPE_p$  and  $n_p$ .

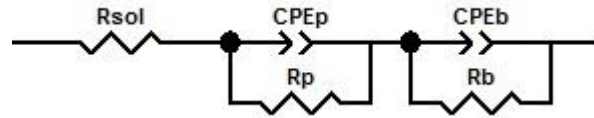


**Figure 4 – Electrical equivalent circuit used to fit the EIS diagrams of the unsealed TSA anodized AA2524 sample after 24 h, 48 h and 72 h of immersion in 0.1 mol.L<sup>-1</sup> NaCl solution**

**Table 1 - Fitted parameters values for the EIS response of the unsealed TSA anodized AA2524 after immersion in 0.1 mol L<sup>-1</sup> NaCl solution**

Immersion time (h)	$CPE_p$ (F.cm <sup>-2</sup> .s <sup>(n-1)</sup> )	$n_p$	$CPE_b$ (F.cm <sup>-2</sup> .s <sup>(n-1)</sup> )	$n_b$	$R_p$ (Ohm.cm <sup>2</sup> )	$R_b$ (Ohm.cm <sup>2</sup> )
24	$2.16 \times 10^{-6}$	0.97	$7.01 \times 10^{-5}$	0.54	$2.75 \times 10^4$	$4.93 \times 10^4$
48	$4.94 \times 10^{-6}$	0.85	$1.85 \times 10^{-4}$	0.54	$2.46 \times 10^4$	$1.74 \times 10^4$
72	$5.06 \times 10^{-6}$	0.86	$1.52 \times 10^{-4}$	0.61	$2.91 \times 10^4$	$1.89 \times 10^4$

In Table 1, the parameter “n” is the frequency dispersion factor and varies from 0 to 1. When “n” is 1 the CPE can be considered as a capacitor and when “n” is 0 it represents a resistor, 0.5 indicates a diffusion controlled process. The CPE values are typical from oxide layers.  $R_p$  remains relatively constant during the whole test period, probably due to the incorporation of deposited products inside the porosities of this layer. This is also most likely the origin of the high  $n_p$  values. The decrease of  $R_b$  until 72 h of immersion associated to the increase in the values of  $CPE_b$  and  $n_b$  (around 0.5), typical of diffusion processes, indicates a strong degradation of the barrier layer.

### 3.2.2 - EIS of hydrothermally sealed or hybrid sol-gel coated TSA anodized AA2524

Figures 5 and 6 show the EIS responses with immersion time in the 0.1 mol L<sup>-1</sup> NaCl test solution of the hydrothermally sealed and hybrid sol-gel coated TSA anodized AA2524 samples, respectively.

Figure 5(a) and 6(a) show that the low frequency impedance modulus of the samples is of the same order of magnitude for the two samples, whereas the phase angle plots, presented in Figure 5(b) and 6(b), display two well defined time constants for both of them during the whole test period, which lasted 42 days. Nevertheless, the low frequency time constant of the hybrid sol-gel coated sample is more capacitive, indicating that the conductive pathways to the sample surface are more difficult. In addition, the high frequency time constant is also more capacitive, indicating better barrier properties.

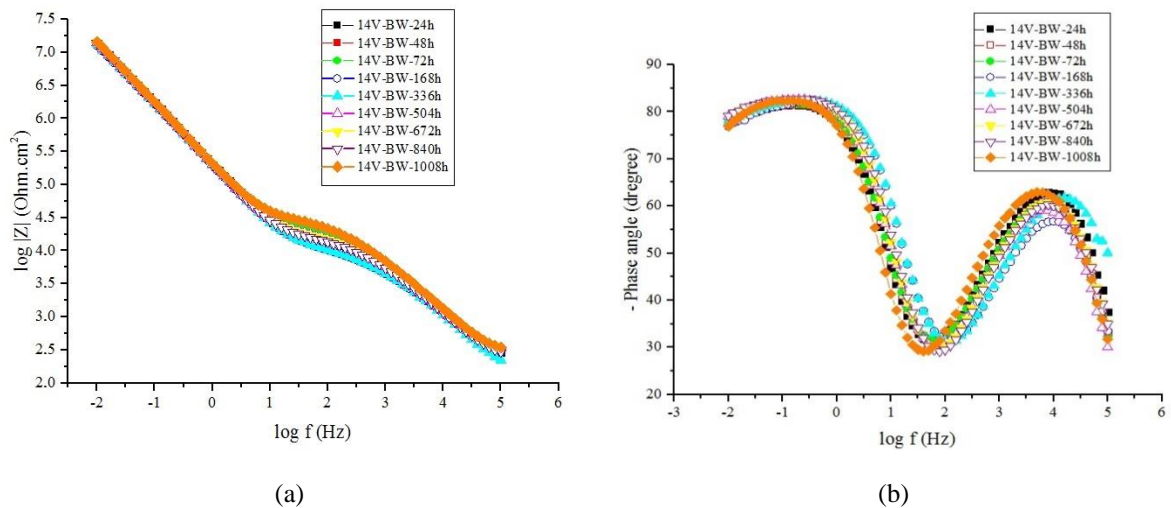


**Figure 5 - Bode plots in (a) Z modulus and in (b) phase angle of hydrothermally sealed TSA anodized AA2524 after different immersion times in 0.1 mol.L<sup>-1</sup> NaCl solution**

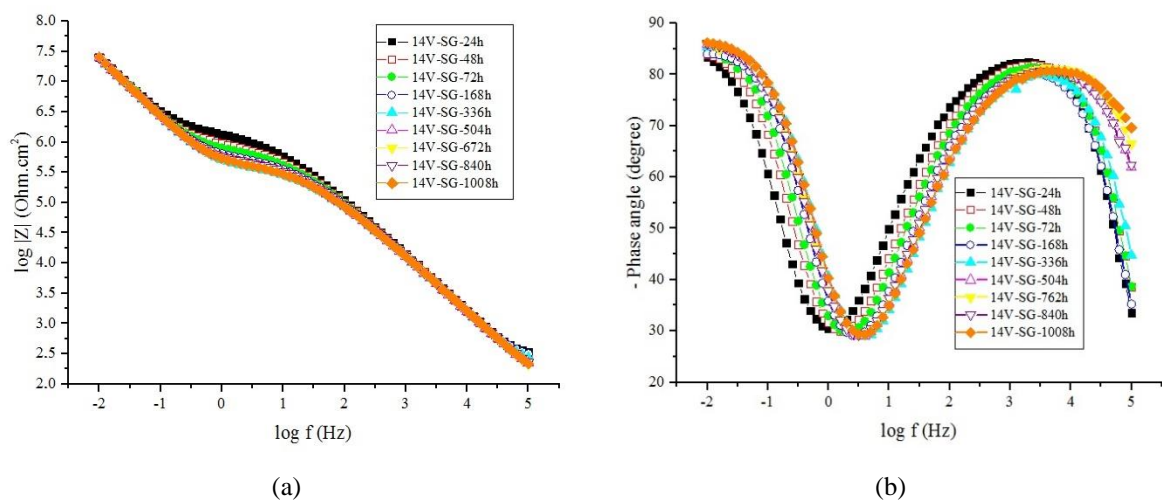


**Figure 6 - Bode plots in (a) Z modulus and in (b) phase angle of hybrid sol-gel coated TSA anodized AA2524 after different immersion times in 0.1 mol.L<sup>-1</sup> NaCl solution**

For the hydrothermally sealed sample, the impedance modulus (Fig. 5 (a)) as well as the phase angle plots (Fig. 5(b)) remain quite stable with time, indicating that there was not much change in the protective properties of the anodized layer due to the contact with the aggressive electrolyte. However, in the medium frequency range of Fig. 5(a) there is slight increase of the impedance modulus with immersion time. González *et al.* (5) published EIS results of anodized pure Al hydrothermally sealed for different immersion times. Their results show that, the longer the sealing time, the higher the impedance modulus in the medium frequency range. Therefore, the increase in the impedance modulus in the medium frequency range showed in Fig. 5(a) indicates that the sealing process continues to take place during the exposure of the anodized sample to the aggressive electrolyte.

For the samples coated with the hybrid sol-gel layer, whereas the low frequency impedance modulus remains relatively constant during the whole test period (Fig. 6(a)) there were huge modifications both in the medium frequency range of the impedance modulus diagram (Fig.

6(a)) and in the phase angle plots (Fig. 6(b)). This indicates that important changes in the properties of the protective layer took place during the immersion period. The diminution of the impedance modulus in the medium frequency range points to the increase in the number of conductive pathways through the hybrid coating and/or to water uptake by the hybrid coating.

In order to have a better insight about the evolution with immersion time of the protective properties of the two post-treated anodized layers, the impedance diagrams were fitted with the EEC presented in Fig. 7. They are similar to those used by Capelossi *et al.* (4) to fit their impedance diagrams for hydrothermally sealed (Fig. 7(a)) and hybrid sol-gel coated (Fig. 7(b)) TSA anodized clad AA2024. In the EEC most of the capacitances were substituted for constant phase elements (CPE) in order to take into account the non-ideality of the system.

In both EEC  $R_{el}$  corresponds to the electrolyte resistance (fitted values not presented).  $C_{pw}$  and  $CPE_{pw}$  are related, respectively, to the capacitive response of the pore walls of the hydrothermally sealed and of the hybrid sol-gel coated anodized layer.  $CPE_p/R_p$  is ascribed to the response of the hydrothermally sealed pores whereas  $CPE_{sg}/R_{sg}$  is attributed to the response of the pores filled with the sol gel coating. Finally,  $CPE_b$  and  $R_b$  are associated with the response of the barrier layer. Before going on with the analyses of the fitting procedure results, it is important to clear some points of the model:

- For both EEC a pore wall resistance ( $R_{pw}$ ) exists in parallel with the pore wall capacitance, however its value is very high and no conductive pathway is developed through this path.
- The aggressive electrolyte only reaches the barrier layer through the pores.
- For the hybrid sol-gel coated anodized layer,  $R_b$  could not be estimated as the time constant of this process is below the lowest frequency used in this experiment. The low frequency time constant is almost capacitive.
- The capacity values associated with pore walls ( $C_{pw}$  and  $CPE_{pw}$ ) were very similar and almost did not change with immersion time, therefore they will not be presented and discussed. In addition the exponent of the  $CPE_{pw}$  element was very close to unit, indicating an almost ideal response.
- For the fitting procedure, the exponent of the  $CPE_p$  element,  $n_p$ , was fixed to 0.5 in order to minimize the errors. In the literature, this low value has been associated with the complex nature of the aluminum hydroxide precipitated within the pores that probably presents a porous structure that could be better represented by a transmission line element (11).

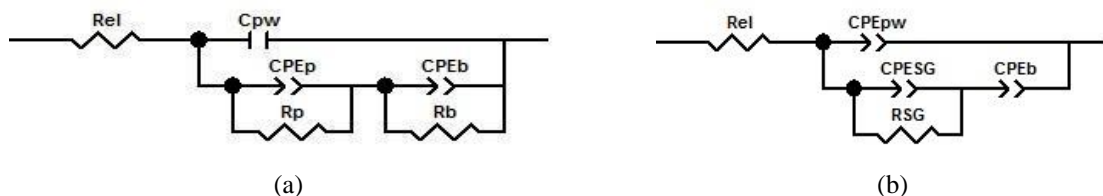


**Figure 7 – Equivalent electrical circuits used to fit the EIS data of the TSA anodized layers hydrothermally sealed (a) and coated with the hybrid sol-gel (b).**

Table 2 presents the results of the fitting procedure for the hydrothermally sealed TSA anodized AA2524. The value of  $CPE_p$ , which exponent was fixed to 0.5, remains almost



constant up to 840 h of immersion (35 d) and then greatly increases for the experiment performed after 1008 h (42 d), pointing to its deterioration.  $R_p$  initially remains almost constant up to 72 h, then decreases up to 336 h (14 d), indicating electrolyte penetration inside the pores, and finally increases again until the end of the experiment. According to González *et al.* (5) the complex sealing and ageing process inside the pores of the anodized layer involves several reactions, which can lead to morphological changes of the precipitated alumina, increasing the resistance of the porous layer. Therefore, this late sealing process can explain the increase in  $R_p$  and is also associated with the impedance modulus increase in the medium frequency range in Fig. 5 (a). Concerning  $CPE_b$ , it remains quite constant throughout the test time and with an exponent close to 1, indicating that it behaves almost like a pure capacitor and that its properties almost does not change. Finally,  $R_b$  remains almost constant up to 336 h and then decreases until the end of the experiment. This behavior can be linked to the response of  $R_p$ . As previously commented, between 168 h and 336 h of test this latter resistance is greatly reduced, which was associated with electrolyte penetration through the porous layer. It is likely that chloride ions penetrating the porous layer reaches the barrier layer surface, starting the corrosion process. The aggressive species will remain trapped underneath the porous layer, and will continue their deleterious action even with the posterior increase of  $R_p$ . Nevertheless,  $R_b$  values remain very high throughout the whole test period, showing that it is a very effective barrier against corrosion. The increase in  $R_b$  value after 1008 h of test can be ascribed to the precipitation of corrosion products within the confined environment of the pores that does not allow easy diffusion of ionic species for the bulk electrolyte.

**Table 2 – Fitted parameters values for the EIS diagrams of the hydrothermally sealed TSA anodized AA2524 sample**

Immersion time (h)	$CPE_p$ ( $\mu F.cm^{-2}.s^{(n-1)}$ )	$CPE_b$ ( $\mu F.cm^{-2}.s^{(n-1)}$ )	$n_b$	$R_p$ ( $k\Omega.cm^2$ )	$R_b$ ( $M\Omega.cm^2$ )
24	1.06	0.895	0.927	26.2	99.0
48	1.12	0.894	0.927	24.4	98.9
72	1.15	0.892	0.927	23.6	99.9
168	1.52	0.926	0.926	12.5	83.7
336	1.45	0.914	0.931	12.3	92.5
504	1.12	0.882	0.936	20.1	11.4
672	1.10	0.890	0.937	19.0	11.8
840	1.09	0.901	0.938	17.2	11.3
1008	0.84	0.868	0.942	34.0	87.4

The results of the fitting procedure for the hybrid sol-gel coated TSA anodized AA2524 are presented in Table 3.  $CPE_{SG}$  slightly increases until the end of the test pointing either to water uptake or to a thinning of the hybrid coating. Its exponent is close to 0.5, indicating a porous nature, likewise the porous layer in the hydrothermally sealed sample. The resistance of the hybrid sol-gel layer,  $R_{SG}$ , steadily decreases, and is reduced to one third of its initial value at the end of the experiment. However, it remains relatively high, in the order of  $M\Omega.cm^2$ , indicating that the electrolyte hardly penetrates through it, and helping to explain why the  $R_b$

value for this sample is below the frequency range investigated in the present work. Finally,  $CPE_b$  remains constant during the whole experiment with an exponent ( $n_b$ ) close to one, indicating that it behaves almost like an ideal capacitor and keeps its properties constants.

**Tabela 3 – Fitted parameters values for the EIS diagrams of the hybrid sol-gel coated TSA anodized AA2524 sample**

Immersion time (h)	$CPE_{SG}$ ( $\mu F.cm^{-2}.s^{(n-1)}$ )	$n_{SG}$	$CPE_b$ ( $\mu F.cm^{-2}.s^{(n-1)}$ )	$n_b$	$R_{SG}$ ( $M\Omega.cm^2$ )
24	0.104	0.474	0.558	0.968	1.77
48	0.118	0.495	0.567	0.965	1.10
72	0.121	0.511	0.566	0.970	0.861
168	0.112	0.552	0.575	0.961	0.609
336	0.156	0.491	0.580	0.968	0.467
504	0.167	0.455	0.575	0.972	0.546
672	0.164	0.457	0.573	0.973	0.574
840	0.180	0.429	0.571	0.974	0.603
1008	0.210	0.409	0.571	0.975	0.528

Figure 8 displays a comparison between the relevant fitted parameters for the hydrothermally sealed and for the hybrid sol-gel coated TSA anodized AA 2524. Figure 8 (a) shows that the resistance of the hybrid sol-gel layer ( $R_{SG}$ ), even though steadily decreasing, remains almost two orders of magnitude higher than the porous layer resistance ( $R_p$ ), indicating a more effective barrier action against electrolyte penetration. Concerning the constant phase element associated with the porous layer ( $CPE_p$ ) and with the hybrid sol-gel layer ( $CPE_{SG}$ ), this latter is almost one order of magnitude lower, indicating that it must be thicker and/or less permeable to water penetration. Finally,  $CPE_b$  for the sample protected with the hybrid sol-gel layer is almost half the value of this same parameter for the hydrothermally sealed TSA anodized layer. Considering that the anodizing procedure was performed using the same parameters for the two samples, it is likely that some hydration of the barrier layer may have occurred during the hydrothermal sealing treatment, increasing its capacitance. However, this process seems to affect neither its stability nor its homogeneity as it behaves almost like a pure capacitor which capacitance does not change with immersion time.

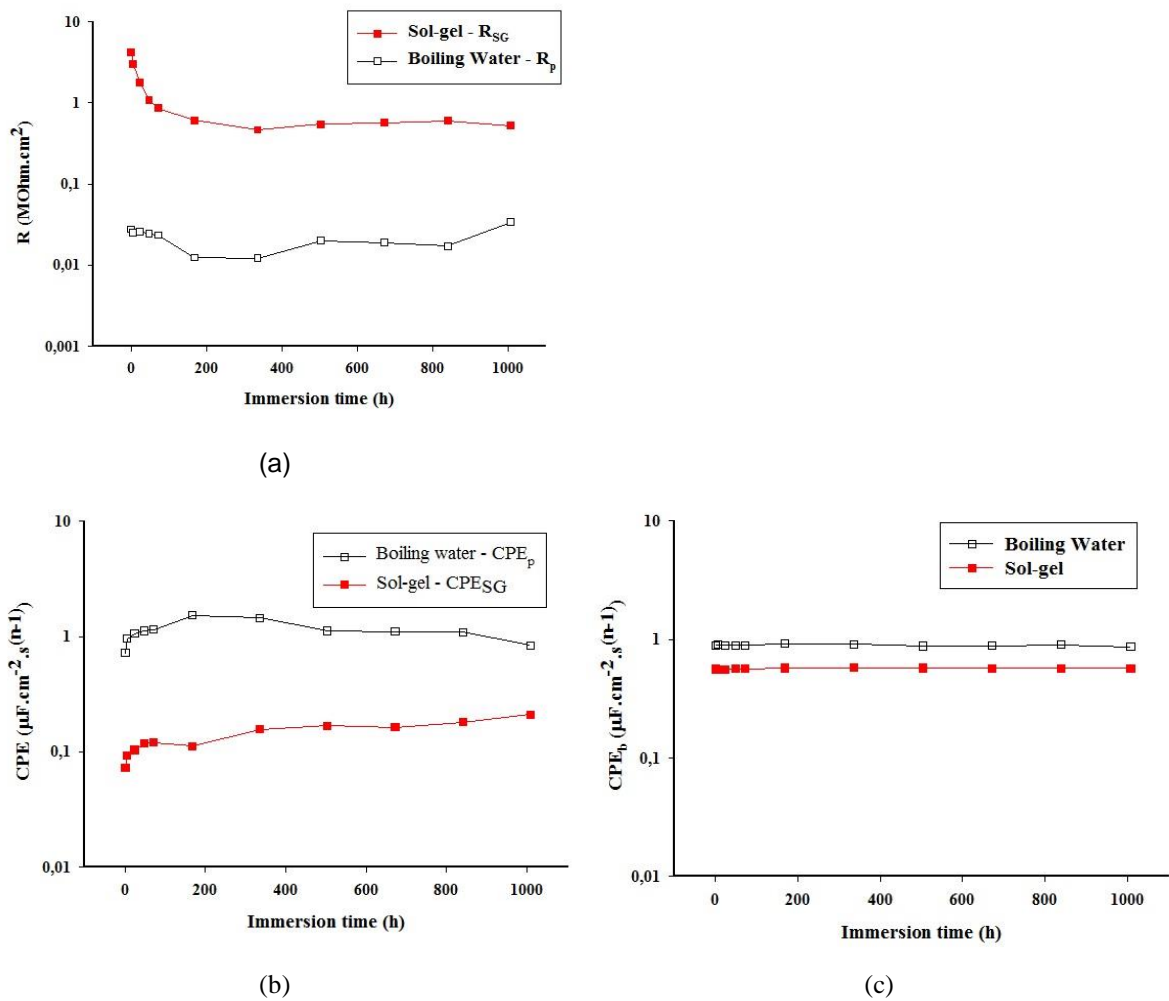
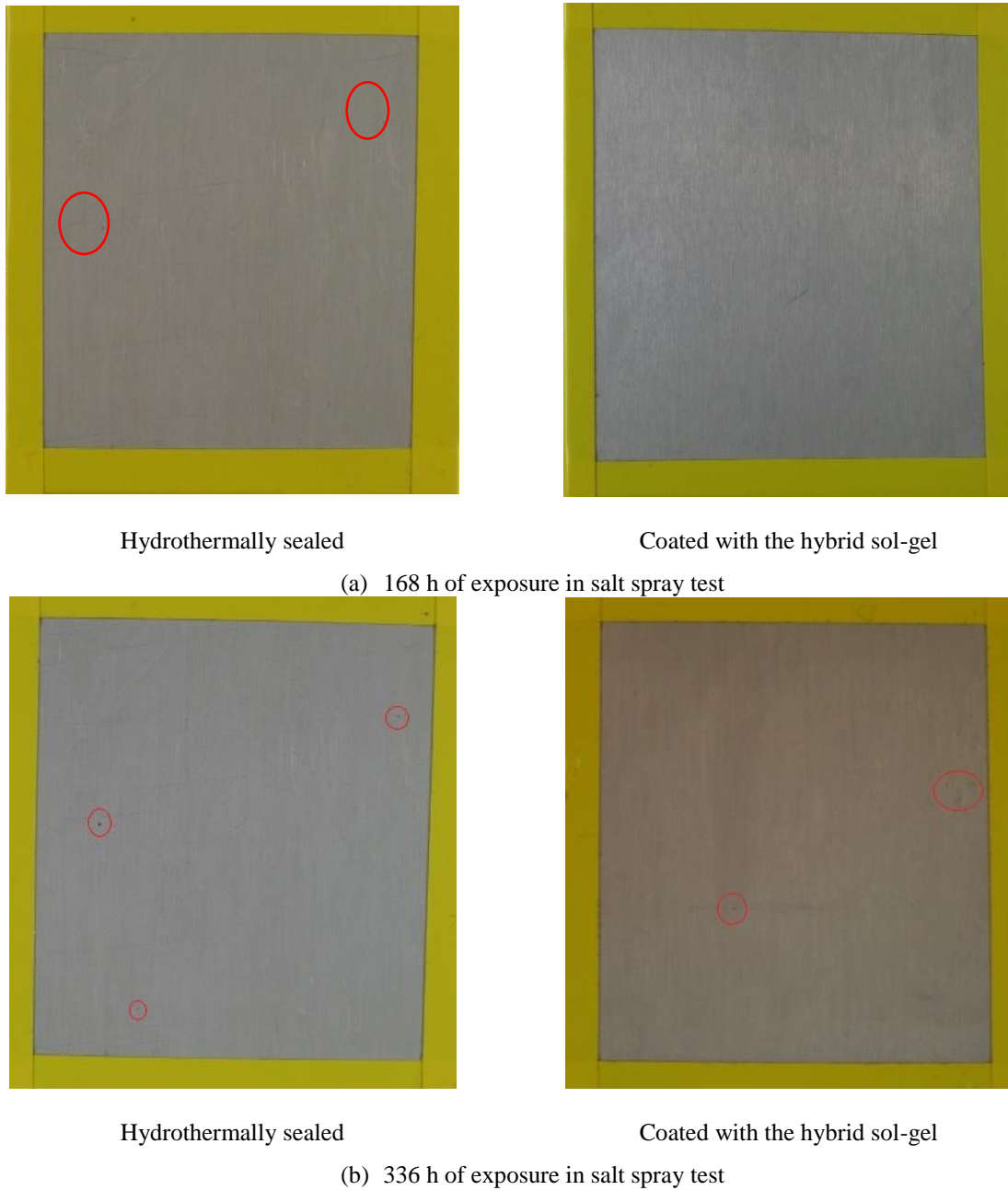


Figure 8 – Comparison of (a)  $R_p$  and  $R_{SG}$ , (b)  $CPE_p$  and  $CPE_{SG}$  and (c)  $CPE_b$  with immersion time for TSA anodized AA2524 protected with the two methodologies.

### 3.3 Salt spray

Salt spray tests were performed in triplicate and according the ASTM B117-11. The samples were observed after 6 h, 24 h, 48 h, 72 h, 168 h, 240 h and 336 h of exposure time. Figure 9 displays the images for 168 h (a) and 336 h (b) of exposure.

Two pits could be observed after 72 h of exposure on the surface of the hydrothermally sealed samples, and 6 pits on the sample coated with the hybrid sol-gel layer (images not shown). The pits on the surface of the hybrid sol-gel coated sample were very small and could not be captured by the camera. After 168 h, pits increased in number and size for the hybrid sol-gel coated sample (not captured by the camera) while for the hydrothermally sealed one, the same two pits observed at 72 h of exposure were seen (Fig. 9(a)).



**Figure 9 – TSA anodized and post-treated AA2524 samples after (a) 168 h and (b) 336 h of exposure to salt spray test**

For longer exposure times (336 h – Fig. 9(b)), pits increased in number and size and were seen on many areas of the hydrothermally sealed sample surface. Most of them were very small and, again, could not be registered by the camera. For the hybrid sol-gel coated sample, no deep pits could be seen, indicating that the hybrid sol-gel post-treatment effectively hindered their growth.

#### **4 – Conclusions**

In the present study, the corrosion behavior of TSA anodized AA2524 samples post-treated either by hydrothermal sealing or with a hybrid sol-gel layer was compared by means of EIS

experiments and salt spray test. The EIS results have shown that the impedance modulus for both types of sample was of the same order of magnitude, however a more capacitive high and low frequency response was observed for the hybrid sol-gel coated sample, indicating greater penetration difficulty to aggressive species and better overall anticorrosion behavior. EEC fitting confirmed this assumption and evidenced that the post-treatment with the hybrid sol-gel layer greatly increases the resistance to electrolyte penetration within the porous layer. This must be the main reason for the superior corrosion resistance of this particular type of sample. These results were supported by the salt-spray test ones, which showed that the sample protected with the hybrid sol-gel layer is less sensitive to the progress of pitting corrosion.

The comparison between two post-treatments for TSA anodized AA2524 revealed that hybrid sol-gel coating is a promising procedure for improving the corrosion resistance of anodized Al alloys.

## 5 - References

- (1) WHELAN, M.; CASSIDY, J.; DUFFY, B. Sol-gel sealing characteristics for corrosion resistance of anodised aluminium. **Surface and Coatings Technology**, v. 235, p. 86 - 96, 2013.
- (2) STALEY, J.T.; LEGE, D.J. Advances in aluminum alloy products for structural applications in transportation. **3rd European Conference on Advanced Materials and Processes**. Paris, jun 08-10, 1993.
- (3) THOMPSON, G. E.; HABAZAKI, H.; SHIMIZU, K.; SAKAIRI, M.; SKELDON, P.; ZHOU, X.; WOOD, G. C. Anodizing of aluminium alloys. **Aircraft Engineering and Aerospace Technology**, v. 71, p. 228 – 238, 1999.
- (4) CAPELOSSI, V. R.; POELMANC, M.; RECLOUXA, I.; HERNANDEZ, R. P. B.; MELO, H. G. de.; OLIVIERA, M. G. Corrosion protection of clad 2024 aluminum alloy anodized in tartaric-sulfuric acid bath and protected with hybrid sol-gel coating. **Electrochimica Acta**, v. 124, pg. 69 - 79, 2014.
- (5) GONZALEZ, J. A.; LOPEZ, V.; BAUTISTA, A.; OTERO, E. Characterization of porous aluminium oxide films from a.c. impedance measurements. **Journal of applied electrochemistry**, v. 29, p. 229-238, 1999.
- (6) ARENAS, M. A.; CONDE, A.; DAMBORENEA, J. J. de. Effect of acid traces on hydrothermal sealing of anodising layers on 2024 aluminium alloy. **Electrochimica Acta**, v. 55, p. 8704 – 8708, 2010.
- (7) GARCÍA-RUBIO, M.; OCÓN, P.; CURIONI, M.; THOMPSON, G. E.; SKELDON, P.; LAVÍA, A.; GARCÍA, I. Degradation of the corrosion resistance of anodic oxide films through immersion in the anodising electrolyte. **Corrosion Science**, v. 52, p. 2219 – 2227, 2010.
- (8) FIGUEIRA, R. B.; SILVA, C. J. R.; PEREIRA, E. V. Organic-inorganic hybrid sol-gel coatings for metal corrosion protection: a review of recent progress. **J. Coat. Technol. Res.**, v. 12, n. 1, p. 1 – 35, 2015.
- (9) ASTM American Society for Testing of Materials, ASTM B117-11 Standard Practice for Operating Salt Spray (Fog) Apparatus, 2012.
- (10) GARCIA-VERGARA, S. J.; KHAZMI, K. EL; SKELDON, P.; THOMPSON, G. E. Influence of copper on the morphology of porous anodic alumina. **Corrosion Science**, v.48, p.2937-2946, 2006.

- (11) BOISIER, G.; PÉBÈRE, N.; DRUEZ, C.; VILLATTE, M.; SUEL, S. FESEM and EIS Study of Sealed AA2024 T3 Anodized in Sulfuric Acid Electrolytes: Influence of Tartaric Acid. **Journal of The Electrochemical Society**, v.155, p.C521-C529, 2008.
- (12) GARCÍA-RUBIO, M.; LARA, M. P. DE; OCÓN, P.; DIEKHOFF, S.; BENEKE, M.; LAVÍA, A.; GARCÍA, I. Effect of posttreatment on the corrosion behaviour of tartaric-sulphuric anodic films. **Electrochimica Acta**, v.54, p.4789-4800, 2009.